# Vehicle Full-State Estimation and Prediction System Using State Observers

Ling-Yuan Hsu and Tsung-Lin Chen

***Abstract*—This paper presents a novel vehicle full-state estimation and prediction system that employs a "full-state vehicle model" together with lateral acceleration, longitudinal velocity, and suspension displacement sensors to obtain the current and future vehicle state information. The full-state vehicle model is a vehicle model with 6 degrees of freedom (DOFs) and is described by 20-state nonlinear differential equations. The proposed approach differs from those in most of the existing literatures in three aspects. First, the road angles and the nonlinear suspension systems are incorporated into the vehicle modeling. Second, the "switching observer scheme" is introduced to significantly reduce the heavy work load that is required for the mathematical derivations. Finally, the full-state vehicle model is employed to predict the vehicle dynamics at future times. The simulation results show that the proposed system can accurately estimate and predict the state values. The relative accuracy of the state estimation is 2.66% on average and 2.86% on average of the state prediction. Furthermore, the proposed system can predict whether the vehicle rollover will occur when a vehicle performs a quick turn on a slope road.**

***Index Terms*—Extended Kalman filtering (EKF), road angles, rollover prediction, state estimation, state observers, state prediction, switching computation scheme.**

## I. Introduction

MANY VEHICLE control systems use current and/or future vehicle state information to improve vehicle stability. Current state information is used to calculate the control input in real time [1], [2], whereas future state information is used to determine the reference trajectory and the times when these control actions should be in effect [3], [4]. The popularity of these approaches highlights the importance of a vehicle state estimation and prediction system that can obtain current and future state information.

Many researchers use "state observer" techniques to obtain current state values because these techniques can effectively reduce the sensor usage [5], [6]. To accurately estimate the state values, the mathematical model of the physical system must be as precise as possible. However, this often leads to a model with high-order nonlinear differential equations. Some of the conventional nonlinear observer design methods, such as the extended Kalman filtering (EKF), require information from the Jacobian matrices of system equations and measurement equations at each sampling time [7]. To construct such an observer for an $n$-state $m$-output nonlinear system, one needs to derive $(n \times n + m \times n)$ equations by hand. For large-scale systems, this is impractical. For this reason, most of the vehicle state estimation systems were developed from simplified vehicle models [1], [5], [8], which means that a significant portion of the vehicle dynamics was neglected. Although they verified the feasibility of their approaches by experimental results, without detailed discussions, the neglect of certain vehicle dynamics may limit the observer design to certain vehicle control applications.

In [9], the author proposed a novel switching computation scheme that can numerically solve the differential equations. With that method, a set of high-order differential equations is first separated into two sets of low-order differential equations. These two sets of differential equations calculate the state values in a way similar to the conventional alternative direction implicit methods [10]. The state values calculated by this method can fairly be close to those of the analytical solutions, depending on the duration of the "switching time." This method can be extended to the nonlinear observer design to greatly reduce the work required for the large amount of equation derivations.

Many methods have been proposed to predict the vehicle rollover, including time-to-rollover [11], rollover velocity [12], genetic algorithm predictor [13], rollover index [14], etc. These methods predict the vehicle rollover by using the current vehicle state values accompanied with heuristic formulas or oversimplified vehicle models. These methods may not be applicable to most cases because the vehicle rollover is a result of multiple vehicle dynamics, vehicle maneuvering, road angles, etc. All of these factors must simultaneously be examined for reliable rollover predictions.

Many researches have shown that the road angles are crucial to the vehicle attitude determination [15], [16]. However, they are still ignored in most of the vehicle control systems. To obtain the vehicle attitude without interference from the road angles, two requirements must be met. First, the road angles must be integrated into the vehicle model so that the model can describe the vehicle behaviors on a slope road. Second, the sensors deployed to measure the vehicle attitude must be capable of excluding the road angles.

The aim of this paper is to construct a database that contains the vehicle "full-state" information at the current and future times for multiple vehicle control applications. The "full-state" information refers to every state value where those states are defined in the "full-state vehicle model." The full-state vehicle model, which was first proposed by [17], is a vehicle model

Manuscript received October 30, 2007; revised April 1, 2008. First published October 31, 2008; current version published May 29, 2009. The review of this paper was coordinated by Dr. S. Anwar.

The authors are with the Department of Mechanical Engineering, National Chiao Tung University, Hsinchu 300, Taiwan (e-mail: lance1214@gmail.com; tsunglin@mail.nctu.edu.tw).

Color versions of one or more of the figures in this paper are available online at http://ieeexplore.ieee.org.

Digital Object Identifier 10.1109/TVT.2008.2008811

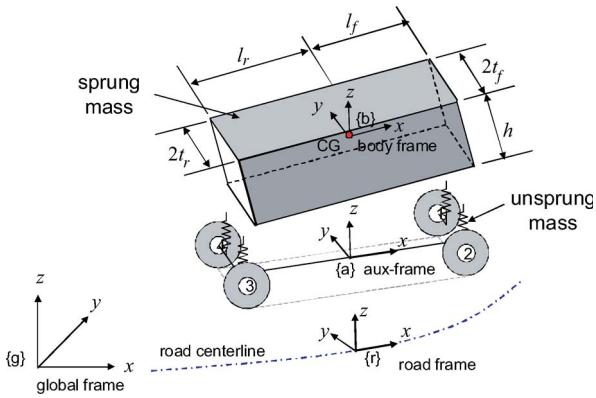


Fig. 1. Four coordinate systems for vehicle modeling.

with 6 degrees of freedom (DOFs) in 3-D space. The vehicle model used in this paper is similar to the model shown in [17] but differs in road angles, suspension dynamics, and engine dynamics. The proposed method in this paper consists of two parts, i.e., the observer-based estimation system and the model-based prediction system. The estimation system is developed by using switching computation techniques. Not only does it reduce the work load required for mathematical derivations but also provides a convenient way of selecting suitable sensors. The prediction system uses a full-state vehicle model and state values from the estimation system to obtain state values at future times, which presents solid evidences for the prediction of the vehicle dynamics. At the end of this paper, the vehicle rollover predictions are used as an example to demonstrate the strength of this method.

The rest of this paper is organized as follows. Section II introduces the four coordinate systems that are used for vehicle modeling. The key features of the proposed full-state vehicle model are discussed in Section III. In Section IV, the switching observer scheme is introduced, followed by the design of the vehicle full-state estimation and prediction system. Section V discusses several system observability issues, and Section VI shows the simulation results. Finally, Section VII concludes this paper.

## II. Coordinate Systems and Euler Angles

Two sets of Euler angles and four coordinate systems (see Fig. 1) are used to construct the vehicle model. These four coordinate systems are the global frame $\{g\}$, road frame $\{r\}$, body frame $\{b\}$, and auxiliary frame $\{a\}$. Similar to conventional approaches, the global frame is fixed to a point on Earth, whereas the body frame is fixed to the center of gravity (CG) of the vehicle. In addition to the conventional approach, the road frame is introduced to describe the vehicle dynamics on a slope road. The relation between the road frame and the global frame is described by the Euler angles $(\psi_r, \theta_r, \phi_r)$, which are referred to in this paper as the "road curve angle," "road grade angle," and "road bank angle." The relation between the road frame and the body frame is described by another set of Euler angles $(\psi, \theta, \phi)$. These three angles can describe the vehicle attitude relative to the road level and are referred to in this paper as the "vehicle yaw angle," "vehicle pitch angle," and "vehicle roll angle." Since the road curve angle does not affect the vehicle dynamics, it is assumed to be zero $(\psi_r = 0)$ in this paper.

The auxiliary frame (aux-frame) is obtained by rotating the $z$-axis of the road frame until the $x$-axis of the road frame is aligned with the $x$-axis of the body frame. The aux-frame is used because it can describe the vehicle translational motions in an intuitive manner while preserving the information of other vehicle dynamics relative to the road level. In the following vehicle model, the vehicle translational motions are described in the aux-frame, whereas the rotational motions are described by the Euler angles $(\psi, \theta, \phi)$.

## III. Vehicle Model

The construction of the full-state vehicle model can be divided into three parts, i.e., sprung mass system, unsprung mass system, and road angles. The sprung mass system describes 6 DOFs of the vehicle body. The unsprung mass system consists of three subsystems, i.e., suspension, tire, and steering systems.

### A. Dynamics of the Sprung Mass System

Similar to other research [18], the vehicle body is assumed to be a rigid body. Using the Euler angles, the rotational motion of the sprung mass can be described as

$$\begin{aligned}
\ddot{\phi} &= \ddot{\psi}\sin\theta + \dot{\psi}\dot{\theta}\cos\theta + \bar{M}_x \\
\ddot{\theta} &= -\dot{\psi}\dot{\phi}\cos\theta + \bar{M}_y\cos\phi - \bar{M}_z\sin\phi \\
\ddot{\psi} &= \dot{\theta}\dot{\phi}\sec\theta + \dot{\psi}\dot{\theta}\tan\theta + \bar{M}_y\sin\phi\sec\theta \\
&\quad + \bar{M}_z\cos\phi\sec\theta \\
\bar{M}_x &= \frac{M_x}{I_x} - \frac{I_z - I_y}{I_x}(\dot{\theta}\cos\phi + \dot{\psi}\cos\theta\sin\phi) \\
&\quad \cdot (-\dot{\theta}\sin\phi + \dot{\psi}\cos\theta\cos\phi) \\
\bar{M}_y &= \frac{M_y}{I_y} - \frac{I_x - I_z}{I_y}(\dot{\phi} - \dot{\psi}\sin\theta) \\
&\quad \cdot (-\dot{\theta}\sin\phi + \dot{\psi}\cos\theta\cos\phi) \\
\bar{M}_z &= \frac{M_z}{I_z} - \frac{I_y - I_x}{I_z}(\dot{\phi} - \dot{\psi}\sin\theta) \\
&\quad \cdot (\dot{\theta}\cos\phi + \dot{\psi}\cos\theta\sin\phi)
\end{aligned} \tag{1}$$

where $M_x$, $M_y$, and $M_z$ are the external torques applied to the CG of the vehicle along the three axes, and $I_x$, $I_y$, and $I_z$ are the moments of inertia of the sprung mass system along the three axes.

As shown in Fig. 2, the Earth's gravity is the only external force acting on the vehicle body that is fixed to the global frame. Therefore, the road angle effect can account for the gravitational force presented in the aux-frame. The three components of the gravitational force, which are represented in the aux-frame ($G_x^a$, $G_y^a$, and $G_z^a$), are

$$\begin{aligned}
G_x^a &= -g(-\sin\theta_r\cos\psi + \cos\theta_r\sin\phi_r\sin\psi) \\
G_y^a &= -g(\sin\theta_r\sin\psi + \cos\theta_r\sin\phi_r\cos\psi) \\
G_z^a &= -g\cos\theta_r\cos\phi_r
\end{aligned} \tag{2}$$

where the superscript $a$ represents the physical quantity observed in the aux-frame. Assuming that the angular rate and

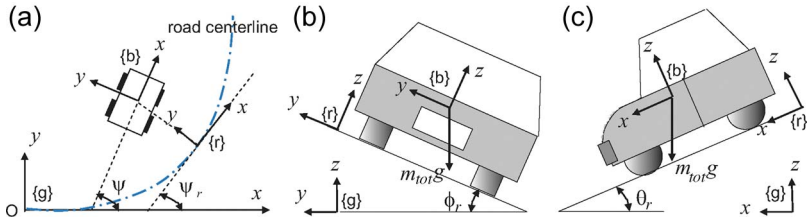


Fig. 2. Vehicles moving on a slope road. (a) Road curve angle $\psi_r$. (b) Road bank angle $\phi_r$. (c) Road grade angle $\theta_r$.

the angular acceleration along the $z$-axis are relatively small ($\dot{\psi}^2 \approx 0, \ddot{\psi} \approx 0$) and using the Newtonian method, the vehicle translational dynamics, which is represented in the aux-frame, can be written as

$$\begin{aligned} m_{\text{tot}}(\ddot{x}^a - \dot{y}^a\dot{\psi}) &= \sum F^a_{x,\text{tire}} + m_{\text{tot}}G^a_x \\ m_{\text{tot}}(\ddot{y}^a + \dot{x}^a\dot{\psi}) &= \sum F^a_{y,\text{tire}} + m_{\text{tot}}G^a_y \\ m_{\text{tot}}\ddot{z}^a &= \sum F^a_{z,\text{spring}} + m_{\text{tot}}G^a_z \end{aligned} \tag{3}$$

where $m_{\text{tot}}$ is the mass of the vehicle; $x^a$, $y^a$, and $z^a$ are the translational displacements of the CG; and $F^a_{x,\text{tire}}$, $F^a_{y,\text{tire}}$, and $F^a_{z,\text{spring}}$ are the net translational forces generated by the tires and suspension systems.

### B. Dynamics of the Unsprung Mass System

*1) Suspension System:* Without loss of generality, the suspension system is modeled as a spring–mass–damper system. Although most of the vehicle models assume a linear dynamics for their suspension systems, this assumption is not applicable to describe vehicle behaviors such as rollover and pitchover. This is because these events are the results of tires lifting off the ground on one end and suspensions reaching their compression limits on the other end. The suspension on the liftoff end generates a force to balance its own weight, whereas the force generated by the other end gradually saturates. For these reasons, a nonlinear spring is used in the suspension system to handle these extreme cases. This leads to the following:

$$\begin{aligned} K_i &= C_1 e^{C_2(H^a_i - C_3)} \qquad (i = 1{-}4) \\ H^a_i &= \begin{cases} H^a_i, & \text{for } H^a_i > -m_{u,i}g/K_i \\ -m_{u,i}g/K_i, & \text{for } H^a_i \le -m_{u,i}g/K_i \end{cases} \end{aligned} \tag{4}$$

where $K_i$ represents the spring stiffness of the suspension corner $i$, and $C_1$, $C_2$, and $C_3$ parameterize the stiffness; $H^a_i$ represents the displacement of the suspension corner $i$; $m_{u,i}$ represents the unsprung mass of the suspension corner $i$; and the subscript $i$ refers to the four suspension corners in a way: $1 \rightarrow$ front left, 2 to 4 in a clockwise motion. When all four tires are on the ground, the suspension displacement is related to the vehicle attitude and the translational motion in the $z$-direction. These relations can be written as

$$\begin{aligned} H^a_1 &= -z^a + l_f \sin\theta - t_f \cos\theta \sin\phi \\ H^a_2 &= -z^a + l_f \sin\theta + t_f \cos\theta \sin\phi \\ H^a_3 &= -z^a - l_r \sin\theta + t_r \cos\theta \sin\phi \\ H^a_4 &= -z^a - l_r \sin\theta - t_r \cos\theta \sin\phi \end{aligned}$$

where $l_f$ and $l_r$ are the distances from the CG to the front and rear axes, respectively, and $t_f$ and $t_r$ are one-half of the distances of the front and rear tracks, respectively. The suspension dynamics, which is represented in the aux-frame, can then be obtained as

$$\begin{aligned} F^a_{z,\text{spring},i} &= K_i H^a_i + D\dot{H}^a_i + m_{u,i}g \qquad (i = 1{-}4) \\ \dot{H}^a_1 &= -\dot{z}^a + l_f\dot{\theta}\cos\theta \\ &\quad + t_f(\dot{\theta}\sin\theta\sin\phi - \dot{\phi}\cos\theta\cos\phi) \\ \dot{H}^a_2 &= -\dot{z}^a + l_f\dot{\theta}\cos\theta \\ &\quad - t_f(\dot{\theta}\sin\theta\sin\phi - \dot{\phi}\cos\theta\cos\phi) \\ \dot{H}^a_3 &= -\dot{z}^a - l_r\dot{\theta}\cos\theta \\ &\quad - t_r(\dot{\theta}\sin\theta\sin\phi - \dot{\phi}\cos\theta\cos\phi) \\ \dot{H}^a_4 &= -\dot{z}^a - l_r\dot{\theta}\cos\theta \\ &\quad + t_r(\dot{\theta}\sin\theta\sin\phi - \dot{\phi}\cos\theta\cos\phi) \end{aligned} \tag{5}$$

where $D$ is the damper coefficient. Note that the suspension displacements ($H^a_{1-4}$) are redundant state variables when the tires are on the ground and independent state variables when the tires are off the ground. This suspension model is one of the major differences from the model proposed in [17].

*2) Tire System:* Using (6), one can link together the tire angular rate, powertrain system, braking system, and adhesive forces as

$$I_{\omega,i}\dot{\omega}^a_i = -r_{e,i}F_{a,i} - T_{b,i} + T_{m,i}, \qquad (i = 1{-}4) \tag{6}$$

where $\omega_i$ is the angular rate of the tire $i$, $F_{a,i}$ is the longitudinal adhesive force generated by the tire $i$, $T_{b,i}$ is the braking torque applied to the tire $i$, $T_{m,i}$ is the traction torque transmitted to the tire $i$, $I_{\omega,i}$ is the moment of inertia of the tire $i$, and $r_{e,i}$ is the effective rolling radius of the tire $i$. The adhesive forces are obtained from Pacejka's magic formula [19], [20], and the associated parameters in the magic formula are excerpted from Feng's dissertation [21]. According to the magic formula, the adhesive force varies with the vertical load on each tire in real time.

*3) Steering System:* The Ackerman steering principle is applied to ensure the smooth cornering of the vehicles. This is done by specifying the angular relations between the steering wheel angle, inner tire angle, and outer tire angle [22]. Once these angles are specified, the adhesive forces in the longitudinal and lateral directions can be obtained. These output forces are then fed into (3) to calculate the vehicle translational motions.

From (1)–(6), one can obtain a 20-state vehicle model that can simulate the highly nonlinear vehicle behaviors on a slope road.

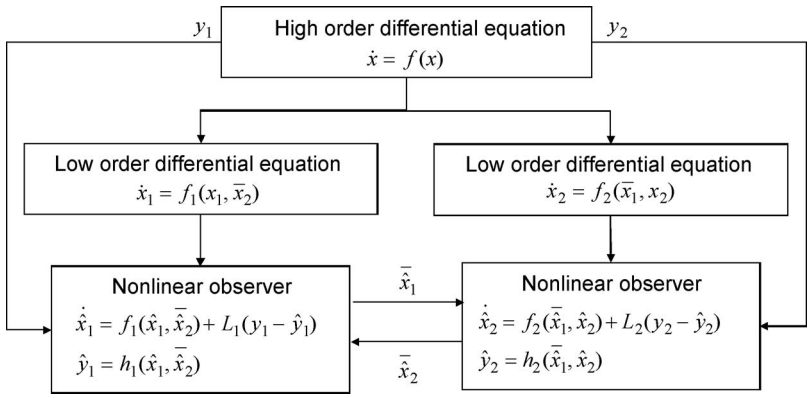


Fig. 3. Schematic of the switching observer scheme. One observer estimates while the other is held static during a switching cycle. They switch their roles of estimating the state values in the next cycle.

## IV. Full-State Estimation and Prediction System

### A. Vehicle Full-State Estimation System

The vehicle full-state information is obtained by using the state observer techniques. As discussed before, using the conventional EKF to construct an observer for this 20-state nonlinear system, one must derive 400 partial derivative terms $(20 \times 20 = 400)$. Moreover, one must derive at least 20 derivative terms to determine the feasibility of a sensor candidate. It is extremely difficult to do so. The switching observer scheme [9] is used to reduce the intensive mathematical derivations in the observer construction and to suggest suitable sensors. In that case, one can then design two individual observers under the switching computation scheme. Each observer requires 100 partial derivative terms, which is much less than the derivative terms required for the conventional EKF.

### B. Switching Observer Scheme

According to the switching computation scheme shown in [9], one set of high-order nonlinear differential equations can be separated into two sets of low-order differential equations. This leads to

$$\dot{x} = f(x) \rightarrow \begin{cases} \dot{x}_1 = f_1(x_1, \bar{x}_2) \\ \dot{x}_2 = f_2(\bar{x}_1, x_2) \end{cases} \tag{7}$$

where $x$ is the state vector of the original high-order differential equation $f(\cdot)$; $x_1$ and $x_2$ are the state vectors of two low-order differential equations [$f_1(\cdot)$ and $f_2(\cdot)$], respectively; and $\bar{}$ denotes the constant values of that state within a switching cycle. If the above high-order differential equations represent the dynamics of a physical system, one can estimate its state values by designing two individual observers for each set of low-order differential equations

$$\begin{aligned} \dot{\hat{x}}_1 &= f_1(\hat{x}_1, \bar{\hat{x}}_2) + L_1(y_1 - \hat{y}_1) \\ \hat{y}_1 &= h_1(\hat{x}_1, \bar{\hat{x}}_2) \\ \dot{\hat{x}}_2 &= f_2(\bar{\hat{x}}_1, \hat{x}_2) + L_2(y_2 - \hat{y}_2) \\ \hat{y}_2 &= h_2(\bar{\hat{x}}_1, \hat{x}_2) \end{aligned} \tag{8}$$

where $\hat{}$ denotes the estimated state value, $y_1$ and $y_2$ represent the sensor measurements, and $L_1$ and $L_2$ are the observer gains. These two observers are operated in a switching computation manner, which means that, in each switching cycle, one observer estimates the state values while the other observer is held static. They switch their roles in the next cycle. A diagram of the switching observer scheme is shown in Fig. 3.

### C. Vehicle Roll Model and Vehicle Yaw Model

Following the preceding discussion, this 20-state vehicle model is separated into two ten-state submodels, which are referred to as the "vehicle yaw model" and "vehicle roll model" in this paper.

Vehicle yaw model

$$\begin{aligned} \ddot{\psi} &= \dot{\theta}\dot{\phi}\sec\theta + \dot{\psi}\dot{\theta}\tan\theta + \bar{M}_y \sin\phi \sec\theta + \bar{M}_z \cos\phi \sec\theta \\ \ddot{x}^a &= \dot{y}^a\dot{\psi} + \sum F^a_{x,\mathrm{tire}}/m_{\mathrm{tot}} + G^a_x \\ \ddot{y}^a &= -\dot{x}^a\dot{\psi} + \sum F^a_{y,\mathrm{tire}}/m_{\mathrm{tot}} + G^a_y \\ \dot{\omega}^a_i &= (-r_{e,i}F_{a,i} - T_{b,i} + T_{m,i})/I_{\omega,i}. \end{aligned} \tag{9}$$

Vehicle roll model:

$$\begin{aligned} \ddot{\phi} &= \ddot{\psi}\sin\theta + \dot{\psi}\dot{\theta}\cos\theta + \bar{M}_x \\ \ddot{\theta} &= -\dot{\psi}\dot{\phi}\cos\theta + \bar{M}_y\cos\phi - \bar{M}_z\sin\phi \\ \ddot{z}^a &= \sum F^a_{z,\mathrm{spring}}/m_{\mathrm{tot}} + G^a_z \\ \dot{H}^a_1 &= -\dot{z}^a + l_f\dot{\theta}\cos\theta + t_f(\dot{\theta}\sin\theta\sin\phi - \dot{\phi}\cos\theta\cos\phi) \\ \dot{H}^a_2 &= -\dot{z}^a + l_f\dot{\theta}\cos\theta - t_f(\dot{\theta}\sin\theta\sin\phi - \dot{\phi}\cos\theta\cos\phi) \\ \dot{H}^a_3 &= -\dot{z}^a - l_r\dot{\theta}\cos\theta - t_r(\dot{\theta}\sin\theta\sin\phi - \dot{\phi}\cos\theta\cos\phi) \\ \dot{H}^a_4 &= -\dot{z}^a - l_r\dot{\theta}\cos\theta + t_r(\dot{\theta}\sin\theta\sin\phi - \dot{\phi}\cos\theta\cos\phi). \end{aligned} \tag{10}$$

Note that this is not the only way of splitting a vehicle system. From the stability analysis of the switching computation scheme, the system (states) splitting can differently be done as long as it satisfies certain stability constraints [9].

### D. Sensor Selections

The lateral acceleration is crucial to vehicle roll dynamics. Therefore, the states that constitute the lateral acceleration must

TABLE I
THREE LARGEST EIGENVALUES AND THEIR ASSOCIATED EIGENVECTOR OF THE OBSERVABILITY GRAMMIAN MATRIX WHEN THE OUTPUT IS LATERAL ACCELERATION

| | Three largest eigenvalues | | |
|---|---|---|---|
| | 42.0533 | 0.1797 | 3.14e-10 |
| Vehicle states | Associated eigenvectors | | |
| $x^a$ | 0 | 0 | 0 |
| $\dot{x}^a$ | -0.0139 | 0.0132 | 0.9998 |
| $y^a$ | 0 | 0 | 0 |
| $\dot{y}^a$ | -0.9780 | 0.2080 | -0.0164 |
| $\psi$ | 0 | 0 | 0 |
| $\dot{\psi}$ | 0.2082 | 0.9780 | -0.0101 |
| $\omega_1$ | -1.70e-05 | 5.04e-06 | 0.0042 |
| $\omega_2$ | -7.09e-06 | 9.15e-07 | -0.0024 |
| $\omega_3$ | -1.62e-07 | -8.94e-07 | -0.0039 |
| $\omega_4$ | 4.97e-08 | 1.77e-06 | 0.0051 |

accurately be estimated to ensure the accuracy of dynamics prediction. Since those states are listed in the vehicle yaw model, we use the lateral acceleration as the output of the vehicle yaw model and examine the resulting observability grammian matrix to reveal the states that are strongly correlated to the lateral acceleration. Furthermore, since the lateral acceleration cannot uniquely be measured, the output of a lateral accelerometer attached to the vehicle CG [see $\ddot{y}_m^g$ in (11)] is utilized instead. The observability grammian matrix is calculated with the linearized yaw model for simplicity. The three largest eigenvalues of the observability grammian matrix and their corresponding eigenvectors are listed in Table I.

Because the first two eigenvalues are much larger than the third eigenvalue, two predominant state combinations are quickly observed. The first two eigenvectors indicate that these state combinations consist of longitudinal velocity $(\dot{x}^a)$, lateral velocity $(\dot{y}^a)$, and vehicle yaw rate $(\dot{\psi})$. Furthermore, the third eigenvalue and its corresponding eigenvector indicate that the observability of the longitudinal velocity is quite low. Therefore, to accurately estimate these three states, one more sensor is needed. Here, we choose the longitudinal velocity sensor $(\dot{x}_m^a)$ as the second sensor. The measurement equations $Y_1$ used in the observer algorithms of the vehicle yaw model are listed as

$$Y_1 = \begin{bmatrix} \left(\ddot{x}^a - \dot{y}^a\dot{\psi} + G_x^a\right)\sin\phi\sin\theta + \left(\ddot{y}^a + \dot{x}^a\dot{\psi} + G_y^a\right)\cos\phi \\ \quad + \left(\ddot{z}^a + G_z^a\right)\sin\phi\cos\theta \\ \dot{x}^a \end{bmatrix} = \begin{bmatrix} \ddot{y}_m^g \\ \dot{x}_m^a \end{bmatrix}. \tag{11}$$

When taking the road angles into consideration, the preferred sensors are those that can measure the vehicle dynamics relative to the road level. For this reason, the suspension displacement sensors are chosen to work with the observer of the vehicle roll model. As discussed before, the suspension displacement $H_i^a$ is either a redundant or independent state depending on whether the tire $i$ is on the ground. Therefore, to accurately estimate all the system states under all situations, we duplicate the measurement equations shown in (12) for the observer algorithms. The duplicated measurement equations share the same values from the corresponding sensor measurements $H_{i,m}^a$. Once a tire is identified to be off the ground, its duplicated equation is removed as it is no longer valid. For example, if the first tire is lifted off the ground, the fifth equation is removed. The measurement equations $Y_2$ used in the observer algorithms of the vehicle roll model are shown as

$$Y_2 = \begin{bmatrix} H_1^a \\ H_2^a \\ H_3^a \\ H_4^a \\ -z^a + l_f\sin\theta - t_f\cos\theta\sin\phi \\ -z^a + l_f\sin\theta + t_f\cos\theta\sin\phi \\ -z^a - l_r\sin\theta + t_r\cos\theta\sin\phi \\ -z^a - l_r\sin\theta - t_r\cos\theta\sin\phi \end{bmatrix} = \begin{bmatrix} H_{1,m}^a \\ H_{2,m}^a \\ H_{3,m}^a \\ H_{4,m}^a \\ H_{1,m}^a \\ H_{2,m}^a \\ H_{3,m}^a \\ H_{4,m}^a \end{bmatrix}. \tag{12}$$

The observer algorithms are chosen to be the EKF because it is simple and effective in the reduction of the sensor noise. Although the EKF has been questioned for its capability of state convergence [7], in that case, one can use an iterative Kalman filter (IKF) to obtain both noise reduction and state convergence. There are several issues of this switching observer scheme, such as state estimation accuracy and system observability. Some of them have theoretically been proven. However, these discussions are beyond the scope of this paper and thus are omitted.

### E. Vehicle Full-State Prediction System

From a system observability viewpoint [23], if both the governing equations of a dynamic system and the state values at an instant in time are given, the state values at any instant in time can accordingly be calculated. Stemming from this concept, one can predict the vehicle dynamics by using a full-state vehicle model and the current state values obtained from the state estimation system.

### F. Block Diagram of the System

Fig. 4 shows a block diagram of the proposed vehicle full-state estimation and prediction systems. The road angles are assumed to be known in this paper. This information and the driver maneuvers, such as steering wheel angle, braking force, and tracking force, are treated as the inputs to the vehicle system and fed into the observer algorithms. The sensor measurements from the three types of sensors (lateral acceleration sensors, longitudinal velocity sensors, and suspension displacement sensors) are fed into the respective observer as well. The switching observer then estimates the state values of the vehicle system in real time. Using these current state values, the prediction system calculates the state values for the next few seconds. In the application of vehicle rollover predictions, the vehicle roll angle at future times can indicate if a rollover incident is likely to occur.

## V. SYSTEM OBSERVABILITY ANALYSIS

The success of state estimation depends on the observability of the system. The local observability of a nonlinear system is determined by the rank of the observability matrix, which

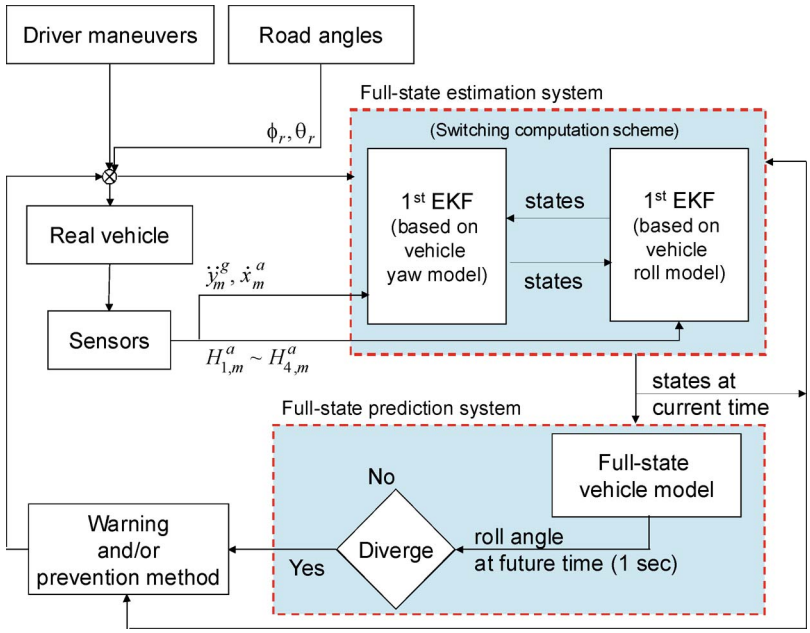


Fig. 4. Block diagram of the vehicle full-state estimation and prediction system.

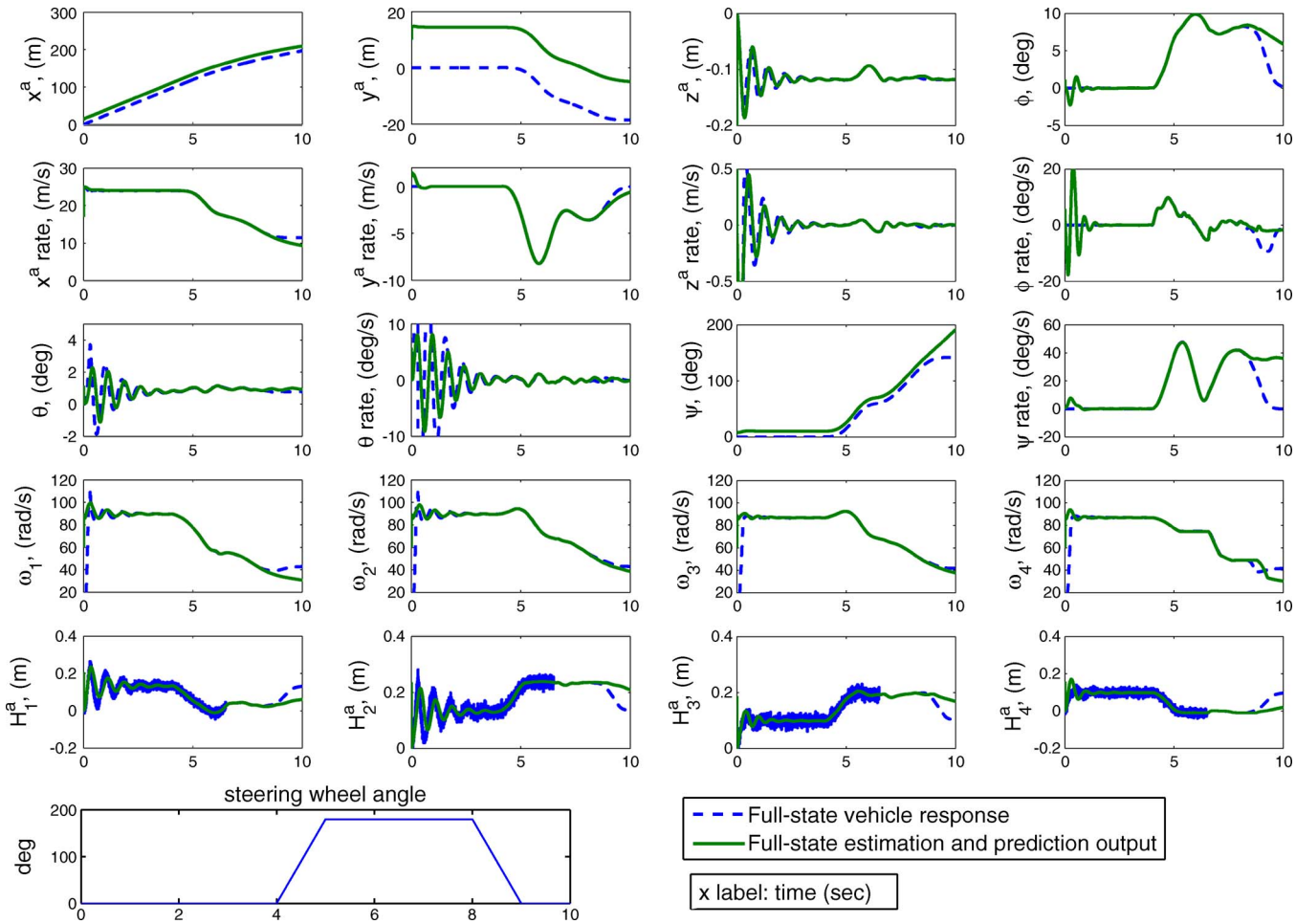


Fig. 5. Case I: The vehicle does not roll over. The estimation system can accurately estimate most of the state values from 0 to 6.5 s. The prediction system can accurately predict most of the vehicle dynamics from 6.5 to 8 s. The estimation and prediction system fails to obtain the state values for the longitudinal displacement $x^a$, lateral displacement $y^a$, and vehicle yaw angle $\psi$.

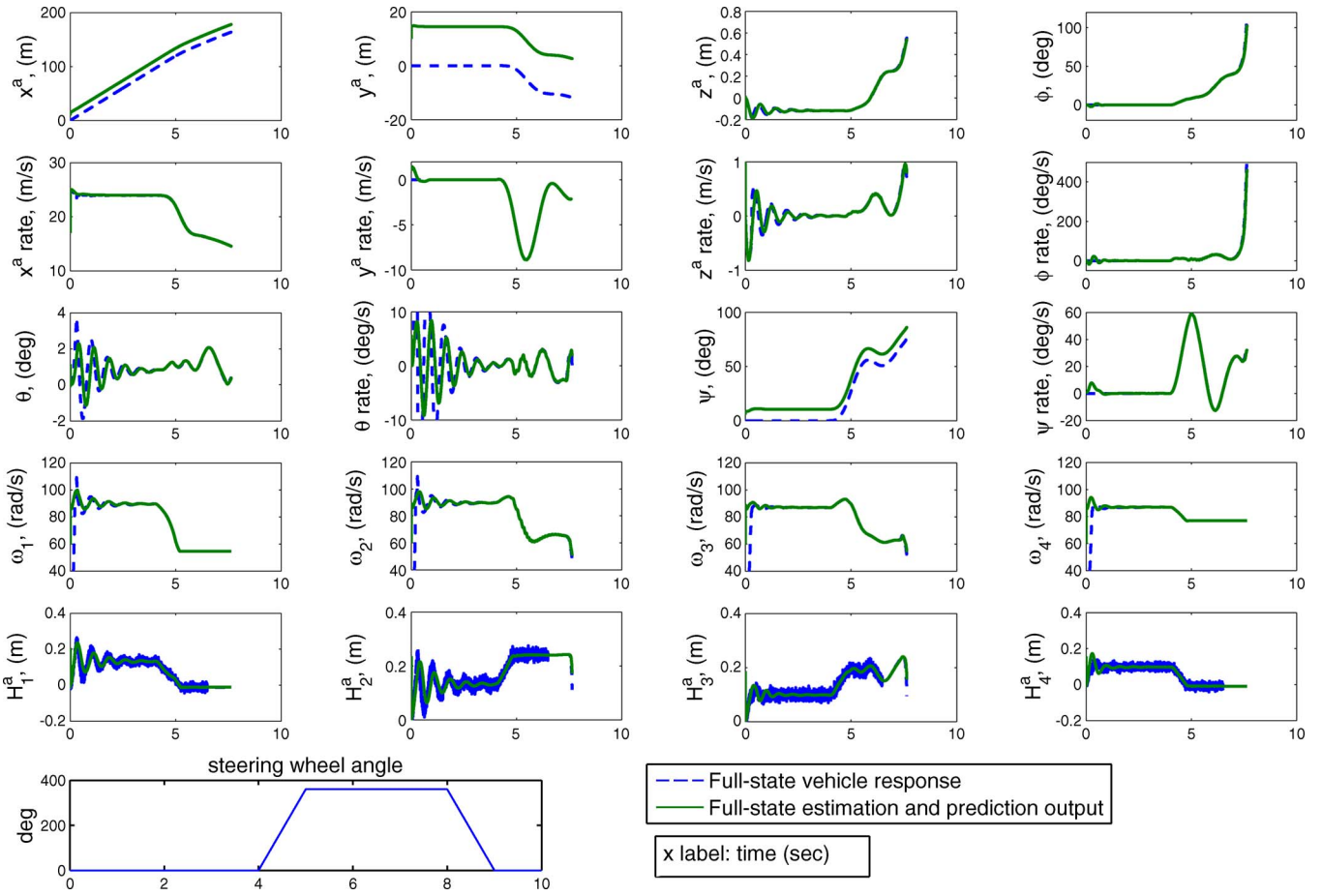


Fig. 6. Case II: Vehicle rollover occurs. The prediction system makes the prediction at the 6.5-s mark and successfully predicts rollover. The estimation and prediction system can accurately obtain most of the state values with the exception of the longitudinal displacement $x^a$, lateral displacement $y^a$, and vehicle yaw angle $\psi$.

is comprised of the gradient of the measurement equations and their derivatives (13) [24]. With the switching observer design, we discuss the observability of the system by separately examining the observability of the vehicle yaw model and the vehicle roll model as

$$W_o = \nabla \left[ Y \quad \dot{Y} \quad \ddot{Y} \quad \cdots \right]^T \tag{13}$$

where the $Y$'s are the measurement equations of a system.

### A. Observability of the Vehicle Yaw Model

Before examining the rank of the observability matrix of the vehicle yaw model, we first check the partial derivatives of the measurement equations [$Y_1$ in (11)] and their derivatives with respect to the states of the longitudinal displacement $(x^a)$ and lateral displacement $(y^a)$ as

$$\frac{\partial}{\partial x^a}\begin{bmatrix} Y_1 \\ \dot{Y}_1 \\ \vdots \\ Y_1^{(n)} \end{bmatrix} = \frac{\partial}{\partial y^a}\begin{bmatrix} Y_1 \\ \dot{Y}_1 \\ \vdots \\ Y_1^{(n)} \end{bmatrix} = \begin{bmatrix} 0 \\ 0 \\ \vdots \\ 0 \end{bmatrix}. \tag{14}$$

Equation (14) reveals that the associated partial derivatives are always zeros, and thus, the longitudinal and lateral displacements are globally unobservable. This result can be understood by the fact that the displacement information cannot be obtained by neither acceleration sensors nor velocity sensors.

Furthermore, the partial derivatives with respect to the vehicle yaw angle $(\psi)$ are also calculated as

$$\frac{\partial}{\partial \psi}\begin{bmatrix} Y_1 \\ \dot{Y}_1 \\ \vdots \\ Y_1^{(n)} \end{bmatrix} = \frac{\partial}{\partial \psi}\begin{bmatrix} 2G_x^a \sin\phi \sin\theta + 2G_y^a \cos\phi \\ 0 \\ \frac{1}{dt}\left(2G_x^a \sin\phi \sin\theta + 2G_y^a \cos\phi\right) \\ G_x^a \\ \vdots \end{bmatrix}. \tag{15}$$

Since $G_x^a$ and $G_y^a$ are functions of $\theta_r$ and $\phi_r$, the elements in (15) are only zeros when $\theta_r = \phi_r = 0$ for the entire trajectory. In that case, the vehicle is moving on a level road, and the vehicle yaw angle cannot be observed from these sensor outputs.

The rank of the observability matrix of the vehicle yaw model is difficult to calculate by hand due to the large amount of mathematical derivations required. In this case, a trajectory of the vehicle states is used to numerically calculate the observability matrix and its rank. The simulation results show that the rank of the observability matrix is seven when the vehicle is moving on a level road and eight when the vehicle is moving on a slope road. According to (14) and (15), these unobservable states are either $(x^a, y^a)$ or $(x^a, y^a, \psi)$, depending on the road

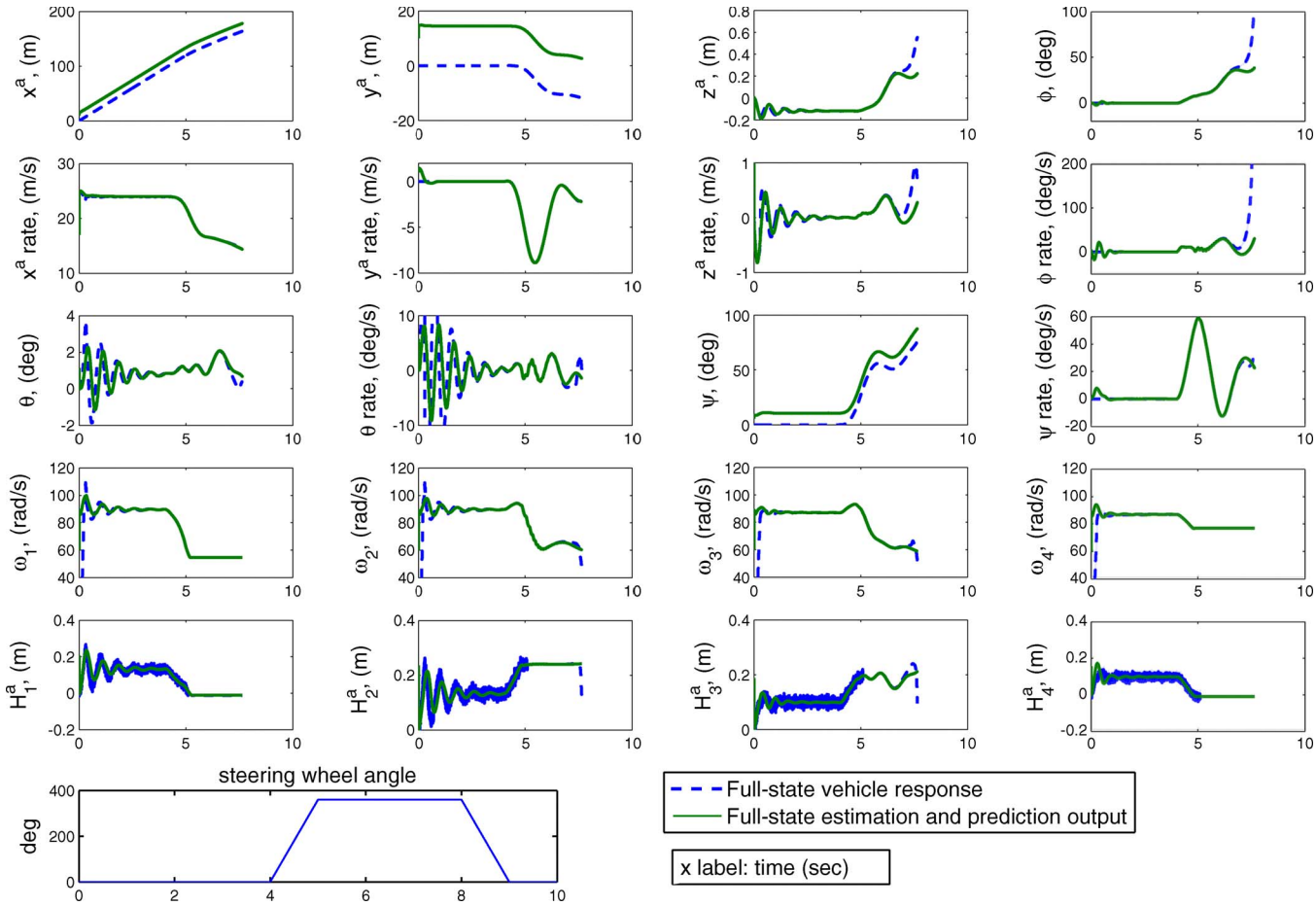


Fig. 7. Case III: Vehicle rollover occurs. The prediction system makes the prediction at the 5-s mark and fails to predict rollover.

angles. Furthermore, since the elements in (14) and (15) are all zeros, the rest of the states in the vehicle yaw model must all be observable. Thus, it is possible to choose a suitable observer algorithm to correctly estimate these state values.

### B. Observability of the Vehicle Roll Model

For simplicity, we check the observability of the vehicle roll model by only using the measurement equations and their first derivatives, which leads to

$$W_{o2} \equiv \nabla \begin{bmatrix} Y_2 \\ \dot{Y}_2 \end{bmatrix} = \begin{bmatrix} 0_{4\times 6} & I_{4\times 4} \\ A_{12\times 6} & 0_{12\times 4} \end{bmatrix}_{16\times 10} \tag{16}$$

where $I$ is the identity matrix. One can show that the lower-left matrix $A$ can provide six independent columns, except when $\theta = 90^\circ$. Thus, all the states in the vehicle roll model can be observed except when the vehicle pitch angle is at $90^\circ$. Furthermore, the derivation also indicates that the rank of the observability matrix can still be ten when two of the duplicated measurement equations in (12) and their derivatives are removed from the observability matrix. This finding suggests that two of the duplicated measurement equations in (12) are redundant for state estimation. However, since it is impossible to know in advance which tire would lift off, all four duplicated measurement equations are used.

### C. Tire Liftoff and Stability of State Estimation

Because the measurement equations in $Y_2$ are excessive, and because the values of $Y_2$ (sensor measurements) are contaminated by noise, the number of local minimums in the estimation process increases. Thus, the nonlinear observer algorithms are likely to converge to wrong values when the vehicle dynamics rapidly change, such as when the tires are lifted off the ground. This problem can skillfully be avoided by removing the duplicated measurement equations in $Y_2$ prior to the tire liftoff. In the following simulations, the duplicated measurement equation is removed from $Y_2$ when the corresponding suspension deformation reaches 85% of its maximum extension. This approach greatly increases the stability of state estimation for unstable vehicle behaviors, such as rollover and pitchover. However, more work is required to investigate this issue.

## VI. Illustrative Simulations

The following simulations are meant to validate the feasibility of the proposed vehicle full-state estimation and prediction method. In these simulations, the vehicle moves at a longitudinal speed of 90 km/h and then makes a left-hand turn at the fourth second. This turn is initiated by a change in the steering wheel angle from the fourth to fifth second. The steering wheel is held at this angle from the fifth to eight second and then switched back from the eight to the ninth second. From 0 to

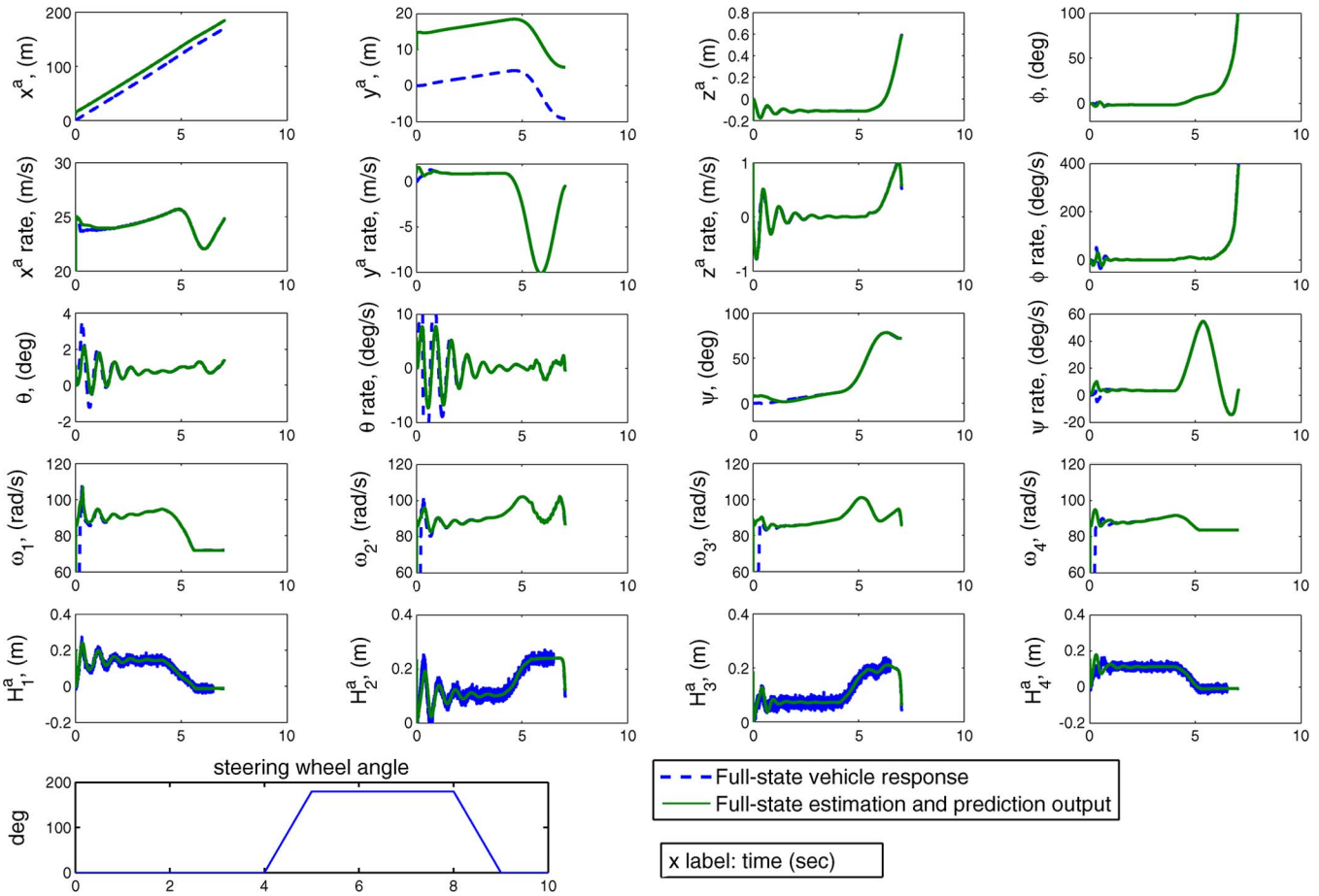


Fig. 8. Case IV: Vehicle rollover occurs due to a road bank angle of $-20^\circ$. The prediction system makes the prediction at 6.5 s and successfully predicts rollover. The estimation and prediction system can accurately obtain most of the state values with the exception of the longitudinal displacement $x^a$ and lateral displacement $y^a$.

6.5 s, the estimated state values are obtained from the switching observers with measurements from three types of sensors. From the 6.5-s mark to the end of the simulation, the estimated state values are obtained from the full-state vehicle model with its initial state values from the output of the switching observer at the 6.5-s mark. Therefore, the estimated state values after the 6.5-s mark can be treated as the output of the prediction system at 6.5 s. Since the steering wheel angle remains unchanged from 6.5 to 8 s, the output of the full-state model should be identical to the output of the prediction system if the prediction system properly functions.

To use EKF for the state estimation, one needs to provide the covariance matrices for the sensor and modeling noises [7]. Without loss of generality, the noise that is associated with each sensor is assumed to be white, independent, and with a standard deviation of 0.01; this leads to a diagonal matrix for the covariance matrix of the sensor noises. The fictitious modeling noise is chosen to have the same properties as the sensor noise for simplicity. Therefore, its covariance matrix is the same as that of the sensor noise except it is scaled by the "sampling time" of the system. The simulation results are shown in Figs. 5–10. The state values from the full-state vehicle model are shown as dashed blue lines and represent the real vehicle dynamics. The state values from the proposed estimation system (from 0 to 6.5 s) and prediction system (from 6.5 s on) are shown as solid green lines. Both the sampling time of the overall system and the switching time of the switching observers are set at $10^{-3}$ s.

Case I shows a vehicle performing a slow turn on a level road. The steering wheel angle changes $180^\circ$ within 1 s; this roughly corresponds to a $10^\circ$ change in the tire angles. As shown in Fig. 5, the vehicle roll angle does not diverge to the applied disturbance when making the turn from the fourth to the fifth second, which means that the vehicle does not rollover as the roll angle is attained within the bound limits. The estimation system can accurately observe most of the vehicle dynamics, and the prediction system can successfully predict most of the vehicle dynamics from 6.5 to the eighth second. The prediction system fails after the eighth second because it is not aware of the change in the steering wheel angle on the eight second. Note that, at the eight second, the prediction system is employing the full-state vehicle model, and the states diverge because no correction action is applied when it is subjected to the system disturbance, such as moving the steering wheel back to center alignment, i.e., $0^\circ$. As expected, the estimation system cannot correctly estimate the longitudinal displacement, lateral displacement, and vehicle yaw angle. Thus, the prediction system fails for these states. The relative accuracy ($\equiv$ (estimated value $-$ real value)/(real value) [25]) of the state estimation is 2.66% on average and 2.86% on average of the state prediction.

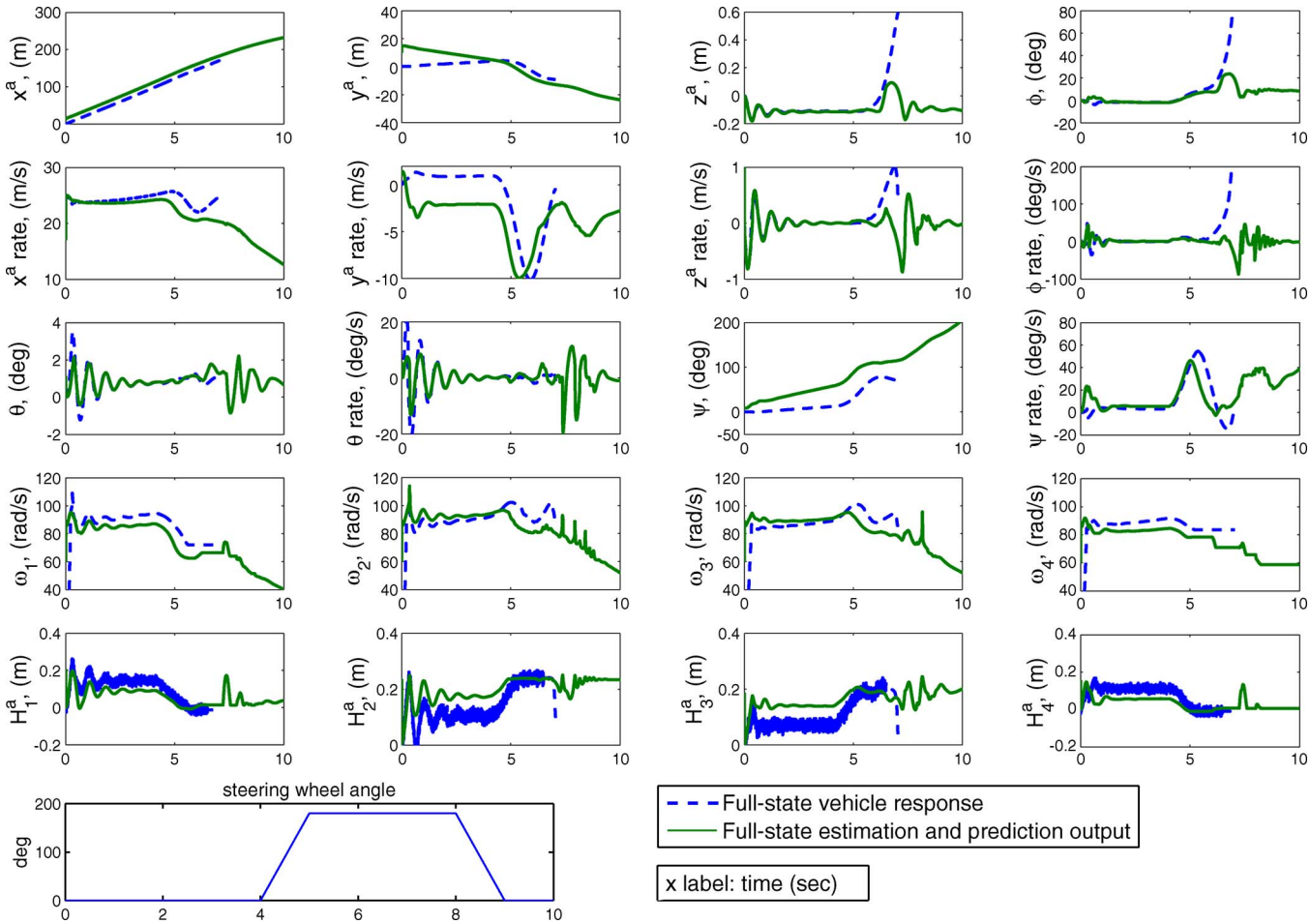


Fig. 9. Case V: The vehicle model does not include road angles. Both the estimation and prediction systems fail to obtain the correct state values.

Case II shows a vehicle performing a quick turn on a level road. The steering wheel angle changes 360° within 1 s; this roughly corresponds to a 20° change in the tire angles. As shown in Fig. 6, the vehicle roll angle diverges, and vehicle rollover occurs. The estimation system can accurately observe most of the vehicle dynamics, and the prediction system can successfully predict the vehicle rollover. Again, the estimations of the longitudinal displacement, lateral displacement, and vehicle yaw angle are erroneous. The relative accuracy of the state estimation is 2.24% on average and 2.78% on average of the state prediction.

Case III shows a vehicle performing a quick turn on a level road while the prediction system predicts the vehicle dynamics with the state values from the output of estimation system on the fifth second. The only difference between Cases II and III is the time when the system makes the prediction. As shown in Fig. 7, the estimation system can observe most of the vehicle dynamics, whereas the prediction system cannot precisely predict the vehicle rollover. This result will be discussed in detail in the next section.

Case IV shows a vehicle performing a slow turn on a road with a bank angle $(\phi_r)$ of $-20°$. The only difference between Cases I and IV is the road bank angle. As shown in Fig. 8, vehicle rollover occurs, and both the vehicle estimation and prediction systems work well. Furthermore, due to the road bank angle, the vehicle yaw angle can correctly be estimated and thus predicted. The relative accuracy of the state estimation is 1.84% on average and 2.07% on average of the state prediction.

Case V shows a vehicle performing a slow turn on a road with a bank angle $(\phi_r)$ of $-20°$, whereas the vehicle state estimation and prediction system excludes the road angles in vehicle modeling. As shown in Fig. 9, neither the estimation system nor the prediction system can obtain the correct vehicle state values. These simulation results show the importance of incorporating the road angles in vehicle modeling.

Case VI shows a vehicle performing a quick turn on a level road with the duplicated measurement equation in $Y_2$ not removed prior to the tire lift off. In this case, the sensors are on at all times, and the line in solid green is the output of the estimation system. As shown in Fig. 10, the state estimation is erroneous when two tires are off the ground at 5.5 s. This simulation result agrees well with the discussion shown in Section V.

### A. Discussion

In this vehicle dynamics estimation system, the three unobservable states are the longitudinal displacement, lateral displacement, and vehicle yaw angle. Therefore, their estimated values are obtained by the integral action over their respective velocity state values. Figs. 5–10 show a deviation between

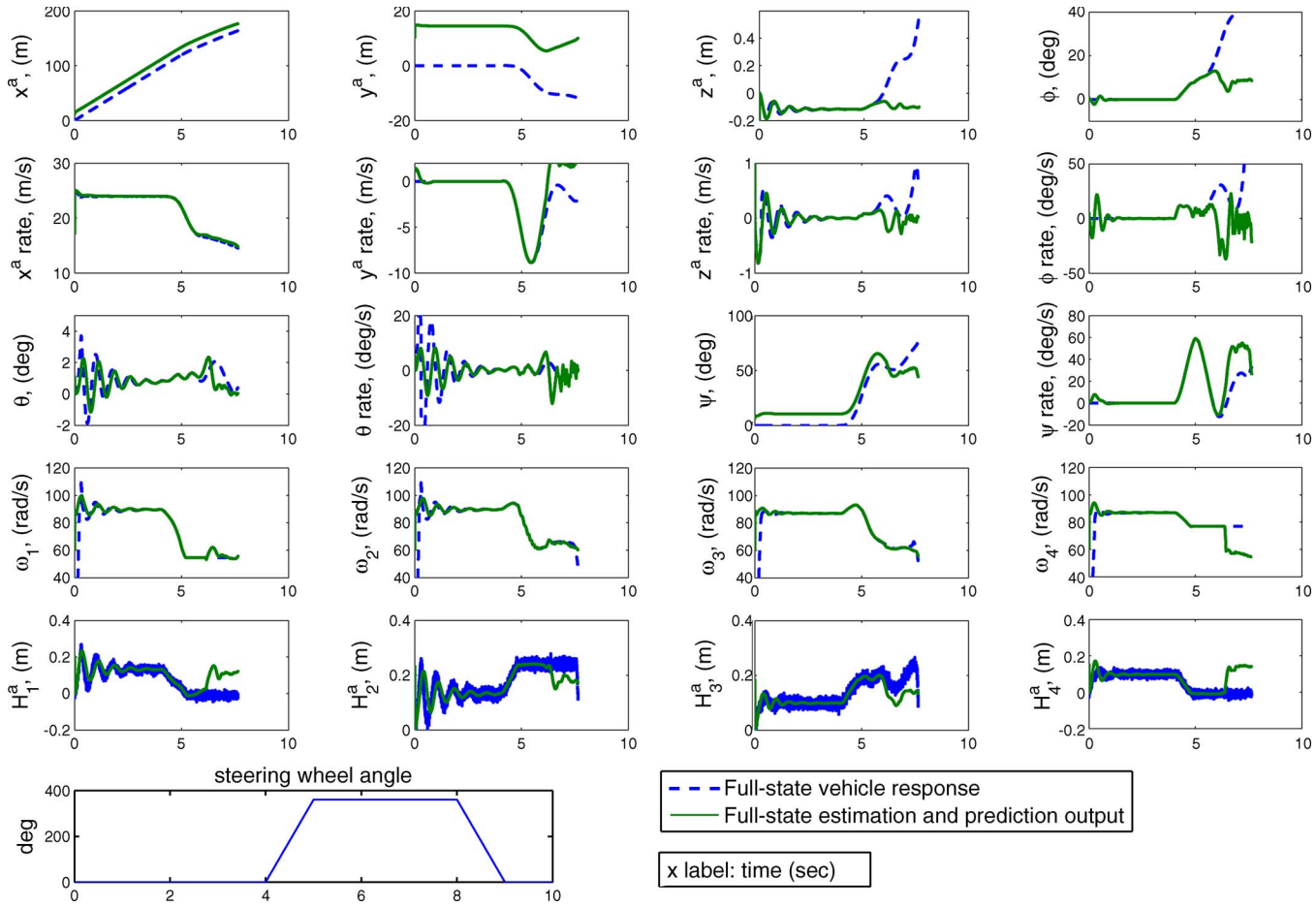


Fig. 10. Case VI: The duplicated measurement equation of suspension displacement in the observer algorithm is not removed prior to tire liftoff. The estimation system fails to obtain the correct state values.

the estimated and correct values for those unobservable states. This deviation can be attributed to the following two sources: 1) unknown initial conditions of those states and 2) estimation errors of their respective velocities. Therefore, although one can reset the vehicle system and obtain correct initial conditions for those unobservable states, the errors of those states could still be large when their velocity state values do not converge to the correct values soon enough.

As can be seen by comparing Figs. 6 and 7, the prediction system can predict the future vehicle dynamics when the state values are obtained from the output of the estimation system at the 6.5-s mark (see Fig. 6). However, it fails when the state values are obtained at the 5-s mark (see Fig. 7). According to the simulation results, the error norm (the deviation between the estimated state values and the state values of the full-state vehicle model) is 0.1261 at 6.5 s and is 0.1843 at the 5-s mark. Since the vehicle rollover is an unstable behavior, and the model-based prediction system is an "open loop" system, a small error in the estimated state values would gradually diverge with time in the prediction system. This explains the different prediction outcomes in the above two cases and thus emphasizes the importance of an accurate state estimation when trying to predict the unstable dynamics. Unfortunately, in the simulation results of the rollover cases (unstable dynamics), the slow divergence between the predicted state values and the real dynamics cannot clearly be shown in the plots. This is because the prediction algorithms got turned off at 8 s due to numerical problems, and the scale of those plots is unable to show small numbers. However, this divergence phenomenon can still be expected from the simulation results that the relative accuracy of the model-based prediction system is always larger than that of the observer-based estimation system, as discussed in each simulation case.

This paper discusses the importance of the road angle effects and assumes that the road angles can be obtained beforehand. Since it is not practical to make such assumptions, the sensors and/or algorithms that can obtain this information are imperative. Equations (2)–(4) show that the road angles do appear in the vehicle model in the aux-frame and that the proposed suspension displacement sensor can measure the state values in the aux-frame. Therefore, it is possible to use suspension displacement sensors and estimation algorithms to obtain the road angles. Because this additional algorithm is beyond the scope of this paper, the related discussions are omitted here.

## VII. Conclusion

In this paper, a vehicle full-state estimation and prediction system has been developed and verified by simulation results. The full-state estimation system is established by using the

switching observer technique along with three types of sensors (lateral acceleration sensor, longitudinal velocity sensor, and suspension displacement sensor). The switching observer technique reduces the amount of mathematical derivations by half. The proposed estimation system can accurately estimate most of the vehicle state values, with the exception of the longitudinal displacement, lateral displacement, and vehicle yaw angle. Furthermore, the success of vehicle yaw angle estimation depends on whether the vehicle is moving on a level road or a slope road. The full-state prediction system uses the full-state vehicle model and the state values from the estimation system to predict the vehicle dynamics in the future. To accurately predict some instability vehicle behaviors, the estimated state values must be as accurate as possible. The proposed state estimation and prediction system achieves a relative accuracy of 2.66% on average of the state estimation and 2.86% on average of the state prediction.

According to this paper, reliable vehicle rollover predictions require the following: 1) the inclusion of road angles in the vehicle model; 2) sensors that are capable of differentiating road angles from vehicle attitude; 3) a suspension model that is capable of describing the nonlinear vehicle behaviors; and 4) sensors and an estimation system that are capable of obtaining correct state values for situations when the tires are both on the ground and off the ground.

## REFERENCES


[1] C. R. Carlson and J. C. Gerdes, "Optimal rollover prevention with steer by wire and differential braking," in *Proc. ASME Int. Mech. Eng. Congr. Expo.*, Washington, DC, 2003, pp. 345–354.

[2] E. N. Scanchez, L. J. Ricalde, R. Langari, and D. Shahmirzadi, "Recurrent neural control for rollover prevention on heavy vehicles," in *Proc. IEEE Int. Conf. Neural Netw.*, 2004, pp. 1841–1846.

[3] E. N. Scanchez, L. J. Ricalde, R. Langari, and D. Shahmirzadi, "Rollover prediction and control in heavy vehicles via recurrent neural networks," in *Proc. 43rd IEEE Conf. Decision Control*, Paradise Island, Bahamas, 2004, pp. 5210–5215.

[4] P. Gaspar, Z. Szabo, and J. Bokor, "Prediction based combined control to prevent the rollover of heavy vehicles," in *Proc. 13th Mediterranean Conf. Control Autom.*, Limassol, Cyprus, 2005, pp. 575–580.

[5] J. Ryu and J. C. Gerdes, "Integrating inertial sensors with GPS for vehicle dynamics control," *Trans. ASME J. Dyn. Syst. Meas. Control*, vol. 126, pp. 243–254, 2004.

[6] Y. Fukada, "Slip-angle estimation for vehicle stability control," *Veh. Syst. Dyn.*, vol. 32, no. 4/5, pp. 375–388, Nov. 1999.

[7] Y. Bar-Shalom, X. R. Li, and T. Kirubarajan, *Estimation With Applications to Tracking and Navigation*. Hoboken, NJ: Wiley-Interscience, 2001.

[8] L. Jianbo and T. B. Allen, "Attitude sensing system for an automotive vehicle," U.S. Patent 6 631 317, Oct. 7, 2003.

[9] L.-Y. Hsu, "Vehicle rollover prediction system using states observers," M.S. thesis, Dept. Mech. Eng., Nat. Chiao Tung Univ., Hsinchu, Taiwan, 2006.

[10] W. H. Hundsdorfer and J. G. Verwer, "Stability and convergence of the Peaceman–Rachford ADI method for initial-boundary value problems," *Math. Comput.*, vol. 53, no. 187, pp. 81–101, Jul. 1989.

[11] B. Chen and H. Peng, "A real-time rollover threat index for sports utility vehicles," in *Proc. Amer. Control Conf.*, San Diego, CA, 1999, pp. 1233–1237.

[12] W. E. Travis, R. J. Whitehead, D. M. Bevly, and G. T. Flowers, "Using scaled vehicles to investigate the influence of various properties on rollover propensity," in *Proc. Amer. Control Conf.*, Boston, MA, 2004, pp. 3381–3386.

[13] V. Trent and M. Greene, "A genetic algorithm predictor for vehicular rollover," in *Proc. IEEE 28th Annu. Conf. Ind. Electron. Soc.*, 2002, vol. 3, pp. 1752–1756.

[14] A. Hac, T. D. Brown, and J. D. Martens, *Detection of vehicle rollover*, Mar. 2004. Soc. Automotive Eng., 2004-01-1757.

[15] J. Ryu and J. C. Gerdes, "Estimation of vehicle roll and road bank angle," in *Proc. Amer. Control Conf.*, 2004, vol. 3, pp. 2110–2115.

[16] H. E. Tseng, L. Xu, and D. Hrovat, "Estimation of land vehicle roll and pitch angles," *Veh. Syst. Dyn.*, vol. 45, no. 5, pp. 433–443, May 2007.

[17] M. Tomizuka, J. K. Hedrick, and H. Pham, "Integrated maneuvering control for automated highway systems based on a magnetic reference/sensing system," California PATH, Berkeley, CA, Res. Rep. UCB-ITS-PRR-95-12, Jan. 1995.

[18] P. Hingwe, "Robustness and performance issues in the lateral control of vehicle in automated highway system," Ph.D. dissertation, Dept. Mech. Eng., Univ. California, Berkeley, CA, 1997.

[19] H. B. Pacejka and E. Bakker, "The magic formula tyre model," *Veh. Syst. Dyn.*, vol. 21, no. S1, pp. 1–18, 1993.

[20] H. B. Pacejka and I. J. M. Besselink, "Magic formula tyre model with transient properties," *Veh. Syst. Dyn.*, vol. 27, no. S1, pp. 234–249, 1997.

[21] K. T. Feng, "Vehicle lateral control for driver assistance and automated driving," Ph.D. dissertation, Dept. Mech. Eng., Univ. California, Berkeley, CA, 2000.

[22] J. W. Grzywna, N. M. Ivano, E. M. Schwartz, and A. A. Arroyo, "KELVIN: A second generation land vehicle," in *Proc. Conf. Recent Adv. Robot.*, 2002, pp. 23–24.

[23] C. T. Chen, *Linear System Theory and Design*. New York: Holt, Rinehart, and Winston, 1984.

[24] M. Vidyasagar, *Nonlinear System Analysis*. Englewood Cliffs, NJ: Prentice–Hall, 1993.

[25] R. Pallás-Areny and J. G. Webster, *Sensors and Signal Conditioning*, 2nd ed. New York: Wiley, 2001, p. 13.


**Ling-Yuan Hsu** received the B.S. and M.S. degrees in mechanical engineering in 2004 and 2006, respectively, from National Chiao Tung University, Hsinchu, Taiwan, where he is currently working toward the Ph.D. degree.

Since 2006, he has been with the Department of Mechanical Engineering, National Chiao Tung University.

**Tsung-Lin Chen** received the B.S. and M.S. degrees in power mechanical engineering from National Tsing Hua University, Hsinchu, Taiwan, in 1990 and 1992, respectively, and the Ph.D. degree in mechanical engineering from the University of California, Berkeley, in 2001.

From 2001 to 2002, he was a Microelectrical-mechanical Systems Design Engineer with Analog Devices Inc. Since 2003, he has been with the Department of Mechanical Engineering, National Chiao Tung University, Hsinchu, where he is currently an Assistant Professor. His research interests include microelectromechanical systems and controls.